

PAPER

Correlation of strontium anharmonicity with charge-lattice dynamics of the apical oxygens and their coupling to cuprate superconductivity

To cite this article: Steven D Conradson *et al* 2024 *Supercond. Sci. Technol.* **37** 025005

View the [article online](#) for updates and enhancements.

You may also like

- [Analysis of structural and electronic properties of Pr₂NiO₇ through first-principles calculations](#)
S M Aspera, M Sakaue, T D K Wungu et al.
- [Regeneration of periapical lesions post-endodontic treatment and periapical surgeries in experimental animals utilizing thermo-responsive nano-tricalcium phosphate/chitosan hydrogel: a proof of concept](#)
Wafa I Abdel-Fattah, Salma Hassan El Ashry, Ghareib W Ali et al.
- [A study of false apical defects in myocardial perfusion imaging with SPECT/CT](#)
N V Denisova and A A Ansheles

Correlation of strontium anharmonicity with charge-lattice dynamics of the apical oxygens and their coupling to cuprate superconductivity

Steven D Conradson^{1,2,*}, Victor Velasco^{3,8,*} , Marcello B Silva Neto³ , Chang-Qing Jin^{4,5}, Wen-Min Li^{4,5}, Li-Peng Cao^{4,5}, Andrea Gauzzi⁶ , Maarit Karppinen⁷ , Andrea Perali⁸, Sandro Wimberger^{9,10} , Alan R Bishop¹¹, Gianguido Baldinozzi¹² , Matthew Latimer¹³ and Edmondo Gilioli¹⁴

¹ Department of Complex Matter, Josef Stefan Institute, 1000 Ljubljana, Slovenia

² Department of Chemistry, Washington State University, Pullman, WA 90164, United States of America

³ Instituto de Física, Universidade Federal do Rio de Janeiro, Caixa Postal 68528 Rio de Janeiro, Brazil

⁴ Institute of Physics, Chinese Academy of Sciences, Beijing 100190, People's Republic of China

⁵ School of Physics, University of Chinese Academy of Sciences, Beijing 100190, People's Republic of China

⁶ IMPMC, Sorbonne Université, CNRS and MNHN, Paris 75005, France

⁷ Department of Chemistry and Materials Science, Aalto University, Aalto FI-00076, Finland

⁸ School of Pharmacy, Physics Unit, Università di Camerino, Camerino 62032, Italy

⁹ Dipartimento di Scienze Matematiche, Fisiche e Informatiche, Università di Parma, 43124 Parma, Italy

¹⁰ INFN, Sezione di Milano Bicocca, Gruppo Collegato di Parma, 43124 Parma, Italy

¹¹ Center for Nonlinear Studies, Los Alamos National Laboratory, Los Alamos, NM 87545, United States of America

¹² SPMS, CNRS CentraleSupélec Université Paris-Saclay, Gif-sur-Yvette F-91192, France

¹³ Stanford Synchrotron Radiation Lightsource, SLAC National Accelerator Laboratory, Menlo Park, CA 94025, United States of America

¹⁴ Institute of Materials for Electronics and Magnetism, CNR, Parma A-43124, Italy

E-mail: st3v3n.c0nrads0n@icloud.com and velasco@if.ufrj.br

Received 20 September 2023, revised 28 November 2023

Accepted for publication 20 December 2023

Published 8 January 2024



Abstract

By means of Cu K edge x-ray absorption spectra of overdoped high-pressure oxygenated superconducting $\text{YSr}_2\text{Cu}_{2.75}\text{Mo}_{0.25}\text{O}_{7.54}$ and $\text{Sr}_2\text{CuO}_{3.3}$, we demonstrate a remarkably strong three way correlation between the superconductivity and the local dynamics of their highly anharmonic Cu–Sr and Cu–apical O pairs. We model the latter as aspects of the Internal Quantum Tunneling Polarons (IQTPs) that give the two-site distributions in extended x-ray absorption fine structure and inelastic pair distribution function measurements. This finding obviates the common assumption that the universal Ba/Sr-apical O dielectric layer, far from only maintaining the separation of charges between the charge reservoir and the CuO_2 conducting domains, plays an unexpectedly active role in the unusual electronic properties of cuprate superconductors. Furthermore, we investigate the effects of the dynamic structure associated with these pairs by means of the exact diagonalization of a prototype Hamiltonian based on a six-atom cluster, with two neighboring Cu–apical O pairs bridged by an anharmonically coupled

* Authors to whom any correspondence should be addressed.

Sr atom and a planar O atom. In terms of the Kuramoto model for synchronization, these calculations show a first order phase transition, driven by anharmonicity, to a synchronized state of the IQTPs, in which a fraction of the charge originally confined to the apical O sites is transferred onto the planar O in the superconducting plane. This combination of experimental results and theory demonstrates that the Ba/Sr-apical O layer of cuprates most likely plays an important role in high temperature superconductivity via its collective charge dynamics.

Keywords: superconductivity, cuprates, polarons, synchronization, EXAFS

1. Introduction

Since the discovery of high-temperature superconductivity (HTSC) in cuprates and related materials [1], decades of intense study have revolutionized branches of condensed matter physics, but have yet to yield a consensus on the origins of the superconductivity. This has led the community to call for new ideas [2–5]. Notably in the search for a universal characteristic, two-site distributions in the dynamic structures of certain Cu–O pairs (figures 1(a) and (b)), coupled to HTSC have been observed in virtually all hole-doped cuprates via extended x-ray absorption fine structure (EXAFS) measurements that probe the instantaneous structure factor, $S(Q, t = 0)$ [6–20]. Concomitant with the original EXAFS report [6], differences between the elastic, $S(Q, \omega = 0)$, and inelastic, $S(Q, \omega > 0)$, structure factors from neutron scattering measurements corroborated those findings [21, 22]. Analogous behavior has also been found in non-cuprate HTSC compounds [23, 24].

These structural anomalies were originally designated *tunneling polarons* [9, 10, 25]. A more precise term differentiating them from Holstein-type and related small polarons is ‘Internal Quantum Tunneling Polarons’ (IQTPs). IQTPs occur when a fraction of the excess charge of a Cu-centered small polaron is localized on one of its neighboring oxygen ions via hybridization to the Zhang–Rice singlet state [26–29]. This decrease in its charge, δ , causes a displacement of the oxygen from its crystallographic position to give a second, distinct Cu–O distance. The IQTP occurs when this localized charge and associated displacement exchange with an identical oxygen ion bonded to this same or an adjacent copper ion via quantum (non-thermal) tunneling at a rate much faster than the host polaron hops to another copper site, confining them within this local cluster (figure 1(c)). Their essential characteristic is this fundamental charge-lattice dynamics that is internal within a small number of neighboring Cu–O pairs. IQTPs are therefore observed as two Cu–O distances in the dynamic structure measured by EXAFS or inelastic neutron scattering, whereas diffraction finds only one [10, 14]. We note that the transformation between static and dynamic structure is not an averaging process because it is not related to static disorder.

The potential significance of IQTPs is that at a critical value of an anharmonic coupling between the two oxygen ions the pairwise exchange of the charge and displacement between them synchronizes, merging the wave functions to encompass the entire cluster built to model their

aspects [30, 31]. This correlated motion of charge and atoms makes IQTPs especially interesting from the perspective that the HTSC driver in cuprates is electron–electron interactions [32–36] that, as found by angle-resolved photoemission spectroscopy (ARPES), are augmented by strongly coupled phonons [37–43]. Other types of measurements [44–51] and calculations [52–54] show the same trend. As a form of direct electron–phonon coupling in which intrinsic quantum oscillations of the atoms between their two sites constitute lattice-assisted dynamical charge transfer, the electron–electron interactions and entanglement that are a consequence of the in-phase oscillations of the Cu–O pairs of the IQTPs provide a conceptual basis for a much more significant role for the lattice. Whether the lattice is involved in the mechanism beyond simply providing a platform for the carriers has been one of the principal issues in HTSC since shortly after its discovery.

An active role for the apical oxygen (Oap) atoms in HTSC has been demonstrated by numerous experiments and calculations. The collective behavior of the charges in the CuO₂ planes that is manifested as the numerous ordered phases poses the same question as the calculations: what are the ramifications of coupling the Oap atoms, which would be linked through the Ba/Sr atoms, as in figure 1? This possibility has been mostly neglected as unlikely because of the absence of any experimental data and the inert charge of the alkaline earth cations [55]. However, it could result in functionality for the entire Ba/Sr–Oap plane in the YBa₂Cu₃O_{7±δ}-type (YBCO) or Bi/Hg/Tl-based compounds and the La_{1-x}Ba/Sr_x–Oap layer in the La₂CuO₄-type (LCO) compounds analogous to the other discrete sections of the structures. This is often referred to as the *dielectric* domain whose function has been presumed to be passively maintaining the separation of the excess holes injected into the CuO₂ *conducting* layers from the *charge reservoir* layer where they originate [56] (figure 1). However, our recent reports on the EXAFS of high-pressure oxygenated (HPO) YSr₂Cu_{2.75}Mo_{0.25}O_{7.54} (YSCO–Mo, $T_c = 84$ K, figure 1) and Sr₂CuO_{3.3} (SCO, $T_c = 95$ K) [57–59] samples, while focused on the Cu–O pairs and their IQTPs, also showed that $\chi(R)$ from the Cu–Sr pair in YSCO–Mo along the *c* axis began to decrease at T_c . This is an anomaly since EXAFS amplitudes are expected to increase with decreasing temperature and thermal motion. The unusual behavior of the Cu–Sr pair raises the question of the possibility of the structural dynamics associated with the dielectric layer possessing a role in the superconducting physics of these systems. Another aspect of the dielectric layer is that, in contrast to the relatively rigid CuO₂ planes and the structures of the charge reservoirs being

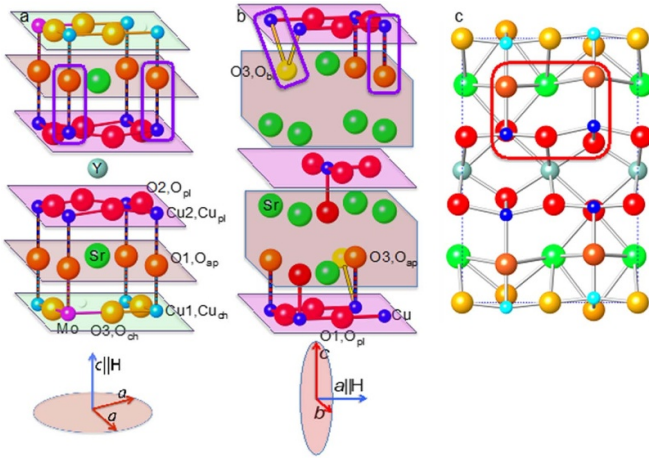


Figure 1. Structures of (a) YSCO–Mo and (b) SCO derived from crystallography and EXAFS, using the standard atom labels from the former. The directions of alignment in a magnetic field are shown at the bottom. The functional domains are: violet = conducting CuO_2 planes; green = charge reservoir layer for YSCO–Mo; beige = dielectric layer that for HPO SCO contains Sr and Oap, but in conventional divalent cation-doped La_2CuO_4 -type compounds is composed of La and the Ca/Sr/Ba. The Mo environment becomes octahedral by incorporating the excess O into neighboring vacancies, introducing a fifth O around adjacent Cu ions. For SCO, half of the O sites between Cu ions along the a direction and many of the Oap sites are vacant. In its dynamic structure we have postulated that the long Cu–O distances are Oap tilting towards adjacent Oap vacancies (yellow), others in red have the short, 1.9 Å Cu–O distance. Cu–O pairs that will form the IQTPs are outlined in purple. (c) The symmetry-allowed atom displacements of the $X2 - (a, 0)$ zone-boundary phonon for YSCO–Mo described below. The displacement magnitudes are arbitrary. The exact diagonalization calculations were performed on the six atom cluster within the red rectangle in which the expanded Cu_{pl} –Oap IQTP exchanges its displacement and $\delta+$ charge with the adjacent contracted Cu_{pl} –Oap IQTP.

those of the parent oxides, the local geometries of the Ba and Sr are highly disordered relative to the rock salt lattices of BaO and SrO .

Although the positive identification of IQTPs is performed by inelastic neutron pair distribution function (pdf) analysis, [21, 60] their coupling to, and role in, HTSC are elucidated by EXAFS [6, 19]. Here, we exploit the capabilities of EXAFS to probe the Cu–Sr pairs and extract changes in their distributions with high precision to advance our findings on the IQTPs in $\text{YSr}_2\text{Cu}_{2.75}\text{Mo}_{0.25}\text{O}_{7.54}$ and $\text{Sr}_2\text{CuO}_{3.3}$ [57–59]. These data are conjugate to vibrational spectroscopy that probes vibrational states via the energies of the collective displacements of atoms in a lattice. Alternatively, the EXAFS signal contains a snapshot of the real space distribution of specific pairs averaged over the probed volume. Anharmonic deviations from Gaussian-like distributions that soften and distort IR and Raman peaks [61] are manifested in the EXAFS as anomalously shaped increases in the normal exponential damping of its pairwise amplitudes in $\chi(k)$ that substantially diminish the magnitude of their Fourier transforms, $\chi(R)$ [11]. Since the quantitative analysis of EXAFS can only be performed if the pair distributions are known, which these obviously are not,

we have adapted an approach that we have used on other systems utilizing direct comparisons of the isolated Cu–Sr components of the spectra. This technique was not performed in our previous reports [57–59].

We find that the Cu–Sr pair distributions along the c axis are not only unusually soft, extending previous reports on their disorder [62, 63] but, surprisingly, they are also highly correlated with both the HTSC and the IQTPs. These results indicate that the entire dielectric domain, both the cations and the Oap atoms, is highly active in HTSC via the local dynamical behavior of its constituent atoms. In addition to these experimental findings, we have performed exact quantum diagonalization calculations on a small cluster (see figure 1(c)) of the structure containing the two Cu–Oap pairs forming the IQTPs bridged by an electronic active Opl site. This introduces the conducting plane in the system, and also a structurally active Sr site coupling the Oap atoms, forming a triatomic Oap–Sr–Oap ‘molecule’. By analyzing the numerical results in the context of the Kuramoto model for synchronization [64, 65], we point to a possible mechanism for the active role of the dielectric domain in the interplay of electronic and structural degrees of freedom of these systems. Moreover, these calculations elucidate the functionality of IQTPs that would underlie an important role for the dynamic properties of these entities in HTSC.

This paper is divided as following: in section 2 we describe the materials and methods used in the experiments. In section 3 we show the experimental results of EXAFS performed in the HPO compounds studied in this work, namely YSCO–Mo and SCO. In section 4 we discuss and show the numerical calculations that supports the interpretation given to the experimental results. Finally, in section 5 we summarize our findings and discuss the implications of our results within the framework of the IQTPs in HPO cuprates.

2. Materials and methods

Descriptions of the materials, sample preparation, and experiments have previously been reported [57–59]. The YSCO–Mo was the same sample used before [66], rechecked to ensure no degradation. The SCO sample was made and characterized for these experiments and consisted solely of the $T_c = 95$ K variant [67, 68] confirmed by XRD and the susceptibility measurements. The grain morphology of HPO cuprates often results in relatively low superconducting fractions [69], but that for the 75 K phase of SCO was stated as $\sim 85\%$ and muon-spin relaxation demonstrates that this is a surface effect, with the actual fraction being $\sim 80\%$ for YSCO–Mo. On this matter, it has been shown both theoretically and experimentally in both cuprates and conventional superconductors that the measured Meissner fraction is highly dependent on the sizes and shapes of the grains, the internal arrangement of their superconducting domains, their packing in the sample, and their conductive connections, with polycrystalline samples usually giving values below $\sim 40\%$ [70–72]. Post synthesis treatments such as a second annealing phase or others have been found to increase this value, leading to the conclusion that Meissner

fractions in this range demonstrate superconducting fractions that are identical to the values obtained for homogeneous superconductivity in single crystals.

The samples were oriented for the EXAFS measurements by suspending the powders in epoxy that was then placed in the bore of a 4–10 T magnet to set and cure. Orientation was confirmed according to [73]. Like all other cuprates, YSCO–Mo is oriented with the c axis parallel to H , while SCO was unique in orienting along an axis perpendicular to the crystallographic c axis that we labeled as a , with the perpendicular direction therefore being the bc plane. The transmission XAFS measurements were performed at the Cu K edge end station 2–2 of the Stanford Synchrotron Radiation Lightsource and its analysis have been described previously in our reports on the local structure at single temperatures [58, 59] and the near neighbor Cu–O pairs over a range of temperatures through the HTSC transition [57].

3. Experimental results

3.1. Data analysis

EXAFS measurements of the two HPO cuprates were performed over a range around T_c to probe their dynamic structure and its coupling to HTSC. The previous reports described the behavior of the Cu–O pairs of the IQTPs, but only examined the temperature dependence of the Cu–Sr χ amplitude in YSCO–Mo without comparing it against any of the other components of the structure. The novel aspect of this paper is therefore the detailed comparative analysis of the IQTP and Sr contributions to the EXAFS over a wide temperature range through the superconducting transitions in both compounds and its ramifications in our calculations. This identifies the surprising strength of the correlation and corresponding coupling to the projection of the Cu–Sr dynamics along the c -axis that was not previously examined.

As stated in the introduction, the quantitative analysis of the spectra in terms of extracting the standard metrical parameters describing the local structure requires *a priori* knowledge of the exact distributions [11]. The difficulty in even assuming a distribution is evident in the complicated behavior of the spectra; the disappearance of the Cu–Oap signal just above T_c in SCO does not lend itself to a determination of a unique pair distribution. An alternative approach for attaining our objective of finding correlations between the pairs and the superconducting transition is the direct comparison of the Cu–Oap and Cu–Sr components of the spectra. Changes in the distributions of the target pairs caused by either shifts of oxygen atoms between different components of their preexisting multisite distributions or originating in their local, pairwise dynamics are then easily identified in the amplitudes of the Fourier transforms, $\chi(R)$, of their isolated contributions to the EXAFS. We have used this for other systems as a method for visualizing trends or patterns in their local structure as a function of an extrinsic variable without having to know the actual shapes of their distributions [74–76].

This separation of the spectral contributions begins with curve-fitting with a harmonic Debye–Waller that validates the structural model by finding the static neighbor shells that conform to the crystal structure and the displaced and dynamic ones that may deviate from it [59]. The contribution of the target pair in $\chi(R)$ is then obtained by subtracting from the EXAFS these waves from those of the other shells of the structure. A critical requirement is the experimental resolution and the confidence that the signal from the target neighbor shell is not affected by and correlated with those of the neighbors that are being subtracted [75, 76]. This becomes especially important in isolating a smaller signal from a larger one with which it overlaps. The resolution of EXAFS is defined as $\Delta = \pi/2k_{max}$ where k_{max} is the highest energy in the analysis [76]; the signature of two shells is the beat in the phase that differs in shape from simple damping from a broad anharmonic distribution. A not uncommon misconception is to relate the resolution to the width of the Fourier transform modulus peaks, in which case the degree of correlation in the signals between neighboring shells would follow from the overlap of their peaks in $\chi(R)$. However, the few to several tenths of an Å width of the $\chi(R)$ peaks is a function of the finite and relatively short total range of the data used in their calculation; the waves for 1.9 Å Cu–O distances complete only six full cycles by $k = 15 \text{ \AA}^{-1}$. That the FT widths are largely an artifact of their calculation is also demonstrated by the use of window functions applied to the $\chi(k)$ spectra that eliminate ripple while broadening the features. All $\chi(R)$ data presented here were calculated with a sine window. For these spectra extending to $k = 15 \text{ \AA}^{-1}$, 0.15 Å separations of the IQTP oxygen shells give a beat at $k = 11.5 \text{ \AA}^{-1}$ that is completely within their upper endpoint. Potential correlation between sets of shells from different elements, e.g. Sr and O, is further reduced by their amplitudes and phase shifts that vary with atomic number.

This process expands the interpretation from a table of metrical results from curve-fits to include a more qualitative visualization of correlations. Analogous to amplitude-ratioing analysis [77], it exploits the extraordinary sensitivity of EXAFS to changes in the pair distributions of closely related samples, e.g. temperature dependence. Not only are the errors in the calculated phases and amplitude and backgrounds canceled, but also the inability to precisely determine disordered structures and unknown pair distributions is rendered less important because the objective is to identify changes. Even if there are errors in the calculated waves of the initial curve-fit that render the metrical data incomplete or with large uncertainties, the essential aspect is the reduction of the contributions of these errors to a level below that where it interferes with the spectral component of interest.

3.2. EXAFS of YSCO–Mo

The Cu K edge $\chi(R)$ of the total structure, the isolated Cu2–Oap contribution, and c -oriented projection of the Cu–Sr pairs of YSCO–Mo from 53 to 110 K are shown in figure 2. These were obtained as described above. The k^3 -weighted spectrum

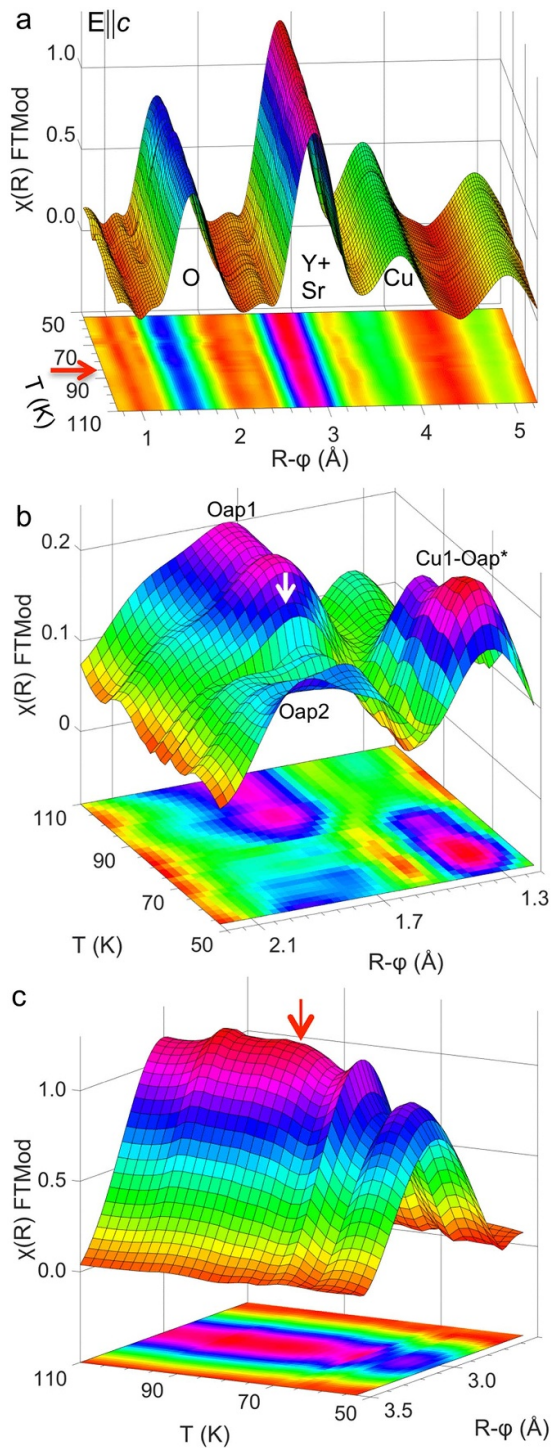


Figure 2. $\chi(R)$ as a function of temperature and position. $R - \varphi$ is used here to indicate that the EXAFS phase shift displaces the modulus peaks from the actual Cu-neighbor positions. (a) Modulus of $\chi(R)$ of the total spectrum showing the neighbor atoms that are the origins of the spectral features. The arrow indicates $T_c = 84$ K. (b) Subtraction of the Cu1-Oap, Y, Sr and Cu-Cu waves from the spectra yields the $\chi(R)$ modulus of the two-site Cu2-Oap IQTP. The contributions of the two Oap sites to the broad or double peak are labeled Oap1 and Oap2. The Cu1-Oap* peak is interpreted as the spectral contribution of an anharmonic component of the Cu1-Oap distribution after subtraction of the Cu1-Oap fit with a Gaussian distribution. (c) Cu2-Sr $\chi(R)$ modulus after isolation by the same procedure.

was curve-fit with the Cu1-Oap, a single Cu2-Oap, Cu2-Y, Cu2-Sr and Cu1-Cu2 neighbors. The curve-fits do not find the Cu1-Sr and Cu2-Cu2 waves, indicating that these pairs are so disordered that they meet the *spectroscopically silent* criteria. This disorder of the Cu2-Cu2 pair is most likely thermal because of the length and presumed poor correlation of the Cu-O-Y-O-Cu link. The absence of the Cu1-Sr contribution would be a more extreme extension of our findings for the Cu2-Sr pair that we discuss below, augmented by the disordered Sr site. All but the Cu2-Oap waves were then subtracted from the total spectra. The residuals were then Fourier transformed to give the results in figure 2(a), with the flatness of the regions $R > 2 \text{ \AA}$ corroborating the negligible Cu1-Sr and Cu2-Cu2 contributions.

The temperature-dependent patterns and trends in the structure, i.e. the absence of any anomalies in the major spectral features and very small change on the high R side of the oxygen peak are much more easily identified in these three-dimensional depictions and are much more easily evaluated than in the original presentation of these spectra as overlays of the moduli. This is especially true for the Cu2-Oap $\chi(R)$ (figure 2(b)). Above T_c , the peak at $R \approx 1.8 \text{ \AA}$ that is the contribution of the Oap with the shorter Cu-O distance is highest. At T_c there is an abrupt drop in its amplitude, followed at lower temperatures by a shift of spectral weight to the $R \approx 2.0 \text{ \AA}$ peak that is assigned to the longer Oap. This plot highlights the extremely narrow width of the change at T_c and the subsequent loss of distinct features over a range below it. A change of the Oap contribution from a double or structured modulus peak to a more symmetric one at the transition is similar to the behavior in other cuprates, although in those cases the cause was identified as a decrease in the separation between the two sites. YSCO-Mo differs from these other compounds in that, instead of recovering the original spectrum there is an obvious shift of spectral weight signifying a shift of some of the Oap from its position closer to Cu2 to the longer Cu2-Oap distance. Another peak at $R = 1.4 \text{ \AA}$ exhibits a distinct increase at T_c . Since this is too short for an actual Cu-O pair, we interpret it as SC-coupled anharmonicity in the Cu1-Oap distribution that does not affect its main peak and is not captured by the fit of this pair with a Gaussian distribution. Similarly, the Cu2-Sr $\chi(R)$ is superior to the previous amplitude ratios in showing the onset of the slow amplitude reduction at T_c followed by the accelerating decrease with decreasing temperature (figure 2(c)).

The metrical data from the curve-fits that provide the additional details that make the essential connection are shown in figure 3. These were obtained by curve-fits of these residuals in which the sum of the numbers of oxygen atoms was fixed. The endpoint of $k = 14.7 \text{ \AA}^{-1}$ gives a resolution of 0.11 \AA . Insofar as the separation between the two oxygen atoms is 0.17 \AA , giving the beat in the composite wave in the EXAFS signifying the two Cu-O distances at $k = 9.3 \text{ \AA}^{-1}$, the Cu2-Oap $\chi(R)$ is not only asymmetric and flattened across its top, but shows two peaks when they are similar in amplitude. The Cu1-Oap distance that is the origin of the large oxygen peak in figure 2(a) is 0.19 \AA shorter than the shorter of the Cu2-Oap pairs, and

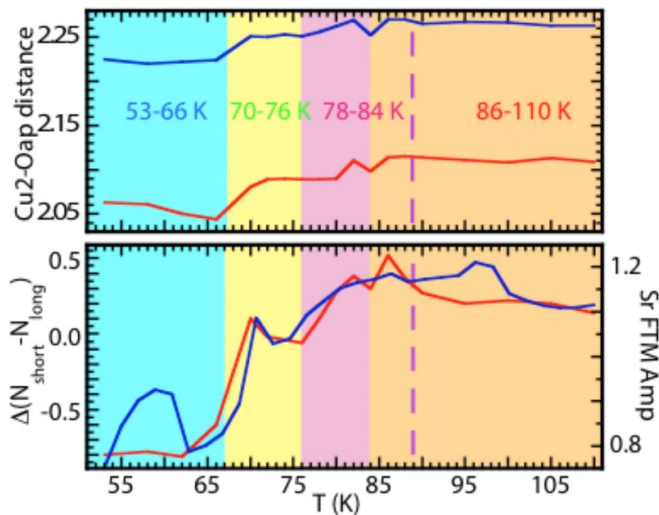


Figure 3. Results for YSCO-Mo. Top graph shows the two independent Cu-Oap distances calculated by curve-fits. They contract in parallel with decreasing temperature. The blue, yellow, and orange zones delineate temperature ranges where these distances are relatively constant. Pink is a fluctuation region that begins at T_c for the distances and somewhat higher (the dashed line) for the numbers of atoms. The red trace in the lower graph shows the difference between the numbers of atoms at these shorter and longer distances that follows the same pattern. The blue trace overlaying the number difference is the amplitude of the c -oriented Cu2-Sr $\chi(R)$ peak in figure 2(c).

the Cu1-Sr is more than 1 Å longer. Being substantially larger than the resolution, the separation is validated. Similarly, although the difference between the Cu2-Y and Cu2-Sr distances is just under the limit and their atomic numbers differ by only one, comparison of their waves from the curve-fits shows that they begin in phase at low energy, as expected, but are π out of phase by the higher energy limit. Insofar as the crystal structure dictates two distinct shells and not a single wide one, the correlation between their signals is therefore negligible and the isolation procedure is effective for the Sr as well.

Our prior analysis of the Cu-Oap pairs found that, based on the two independent Cu-O distances and numbers of atoms, the IQTPs exhibit identical patterns of plateaus and discontinuities at the same temperatures. These delineate the normal phase, a fluctuation region at the transition, and two separate regions in the superconducting phase. Reproducing them here with the addition of the Sr $\chi(R)$ amplitude to the difference in the numbers of oxygen atoms accentuates the novel finding that the peak of $\chi(R)$ displays a remarkable correspondence with the shifts of the two oxygen atoms between their two sites, as shown in figure 3. This even includes the feature at 70 K that would be assigned to a noise spike if it only occurred in one of these results. We emphasize that nothing in the data analysis would bias this correlation between these three parameters and the superconducting transition. The c -oriented $\chi(R)$ peak for the Cu2-Sr (figure 2(c)) is relatively flat at higher temperature, and then begins a slow curve downward at T_c that subsequently

drops more steeply, albeit with some additional features. This behavior is indicative of increasing disorder with decreasing temperature, the opposite to the conventional thermal broadening of the distribution. The correlation is with the difference in the populations of the two Cu2-Oap sites caused by changes in the relative energies of the two minima of the potential (figure 3). The high level of correlation demonstrates the direct coupling of the anharmonicity of the Cu2-Sr distribution to the renormalization of the Cu2-Oap potential and both of these to the SC, including the division into the four regions.

3.3. EXAFS of SCO

Although its composition and parent structure are simple, the EXAFS and local structure of our second material, SCO, are much more complicated than those of YSCO-Mo. A notable aspect is the large changes in the amplitudes with temperature. These are often opposite to the normal reduction with increasing temperature, and several occur over narrow ranges both in proximity to and away from the HTSC transition. Also remarkable is the broad peak at $R = 2.0\text{--}2.8$ Å that does not correspond to sites in the crystallographic structure (figure 1) that vanishes and then abruptly reappears at its maximum amplitude at T_c (figure 4(a)). The magnitude of this change is unprecedented. Our earlier study of SCO found that it is unique among cuprates in exhibiting oxygen vacancies not only in its apical positions but also in its CuO₂ planes. That the planar vacancies occupy approximately half the sites on only one axis provides an explanation for why its alignment in a magnetic field is along that direction instead of its c axis. Because of this rotated magnetism, the Cu-O IQTP in SCO is observed in its crystallographic bc plane [58].

We originally postulated that the behavior of the spectra across the transition might include a strontium atom with a Cu-Sr distance less than 3 Å [57]. However, visualizing the affected spectral region by the isolation method now shows that the large amplitude features at $R = 2.2\text{--}2.8$ Å are present above as well as below the transition. The broad, flat top of this feature from 85–95 K (figure 4(b)) assigns it to the two-site Cu-O distribution characteristic of IQTPs. The remarkable result is its disappearance at T_c , signifying a radical change in the dynamic structure coupled to the superconducting transition, a finding not only outside of BCS superconductivity, but also for HTSC. The absence of a correlation between the amplitudes of the two contributions to the peak is also unique. The current best model for this behavior is that the IQTP oxygen atoms are most likely apical, next to an apical vacancy, displaced along the b axis to asymmetrically bridge two copper atoms at ~ 2.66 and 2.91 Å. Both these distances and the 0.25 Å separation are much longer than any other cuprates. The radical difference in the copper geometries relative to other cuprates, including Opl-Cu-Oap angles lower than 90 degrees, could be a consequence of the much higher copper valence in this overdoped compound. The oxygen atom below them in the b -oriented Cu-O chain shifts away from this Oap to slightly expand its Cu-O bonds [57]. The IQTP could then

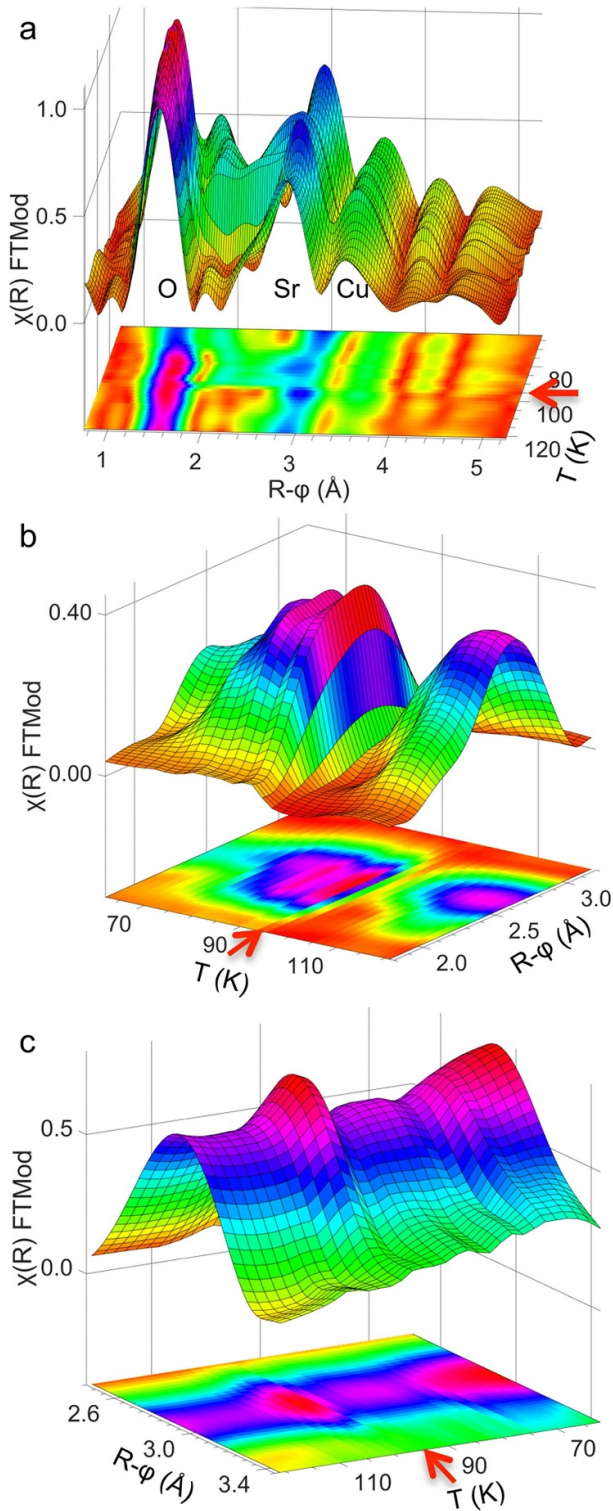


Figure 4. $E||bc$ SCO Cu EXAFS. $R - \varphi$ has the same meaning as in figure 2. (a) Modulus of $\chi(R)$ of the total spectrum labeling the neighbor atoms that are the origins of the spectral features assigned to crystallographic sites. The arrow indicates the transition temperature $T_c = 95$ K. (b) Subtraction of the Cu–O, Sr and Cu–Cu waves from the spectra yields the $\chi(R)$ modulus of the two-site Cu–Oap IQTP as described in the text. The contributions of the two Oap sites are evident in the broad peak below T_c , although they do not track together except for the loss of the total feature just above the critical temperature. (c) Cu–Sr $\chi(R)$ modulus after isolation by same procedure.

include tunneling of the oxygen atoms into equivalent sites across the ac plane that passes through the midpoint of the two coppers as well as between the bridging and vacancy sites. $\chi(R)$ at 121 K in the normal phase has most of its amplitude in the peak for the longer Cu–O distance, with the shorter oxygen giving just a shoulder. The almost complete loss of amplitude at T_c could result from either the separation between the two sites decreasing to maximize the interference of their EXAFS waves and/or their distributions broadening in the fluctuation region of the transition. Below T_c , the two contributions from the two sites are equal. They begin to fall off at ~ 80 K, with the higher R peak again being larger. Repeating, a possible explanation for the diminished overall amplitude of the IQTP at lower temperature is that in this postulated configuration for SCO the oxygen could shift to a normal Oap position directly above the copper along the c direction.

The Cu–Sr contributions were fit with two strontium neighbors at ~ 3.23 and 3.36 Å. This 0.13 – 0.14 Å separation is only marginally larger than the resolution for the $k = 14.2$ Å $^{-1}$ upper limit of the curve-fit. In combination with the disorder that also drives the amplitude down at high k , the increase in the amplitude after the beat will be minimal and the Cu–Sr waves in $\chi(k)$ will be indistinguishable from a single, highly damped one. What is clearly observed now that was obscured in our prior report is that $\chi(R)$ shows a single, round peak with minimal structure. The Cu–Sr $\chi(R)$ amplitude rises as the temperature is lowered from ~ 78 K, also developing a more distinct shoulder on the high R side, where the second strontium at the longer distance needed for a complete curve-fit makes its contribution. This relatively normal trend is broken by the peak beginning near 106 K that falls immediately at T_c , reflecting a narrowing and hardening of the Cu–Sr distribution in the fluctuation region that is eliminated on becoming superconducting. All of these changes can be presumed to originate in the shape and resultant ordering within the single peaked Cu–Sr distribution.

Because of the difficulty of curve-fitting to extract metrical parameters when the features have vanished from the spectra, the correlation with the strontium is derived from comparing the isolated $\chi(R)$ peaks from the IQTP oxygen and strontium atoms at, respectively, $R = 2.6$ and 2.95 Å. The novel result is the high degree of correlation, or in this case anti-correlation, between the Cu–Sr and the IQTP $\chi(R)$ (figure 5), most notably the dramatic response to the onset of the HTSC. As with the YSCO–Mo, the oxygen atoms of the IQTP and the strontium are strongly coupled both to each other and the HTSC. This new analysis therefore shows that the entire putatively inert dielectric layer is actually very strongly coupled to HTSC in SCO.

4. Model calculations

Our demonstration of an anomalous Cu–Sr distribution that is strongly correlated with both the dynamical structure of the Cu–Oap and HTSC poses the questions of the interaction of the strontium with the IQTPs and more generally the HTSC–lattice coupling. We have explored this by applying exact

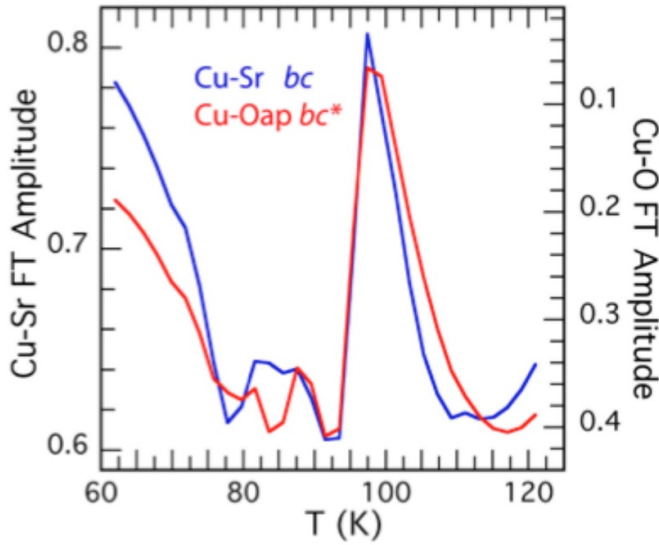


Figure 5. $E||bc$ SCO $\chi(R) \cdot \chi(R)$ modulus amplitudes of the isolated Sr and IQTP O, * = the FT modulus amplitude at $R = 2.6$ Å. The inverse behavior of the two features is apparent.

quantum diagonalization to a six-atom cluster (figure 1(c)) that is an extension of the original, three atom O–Cu–O moiety previously used to elucidate the experimental signatures of IQTPs in the elastic and inelastic structure factors [10, 26]. Briefly summarizing the results of the calculations emphasizes the importance of the strong anharmonic coupling of the strontium to the IQTPs found in EXAFS and its possible or even likely role in the HTSC mechanism.

The minimal subunit encompassing the relevant constituents consists of a pair of neighboring Cu–Oap IQTPs bridged between their copper ions by an Opl and between their Oap by the strontium of the dielectric layer (figure 1) [30, 31]. The novel aspects enabled by this structure are the addition of the CuO_2 plane through the inclusion of Opl and the anharmonic structural dynamics of the Cu–Sr pair that is incorporated via the nontrivial Oap–Sr–Oap triatomic molecular structure indicated by these EXAFS results. In addition to the two localized charges in the Cu sites, a single extra hole initially localized on one of the two Oap atoms causes its displacement to give the two-site distribution. The starting point for the calculation is to consider this cluster as a classic Holstein-type polaron in which a significant fraction of the excess charge is found on one Oap. The standard Hubbard–Holstein Hamiltonian used to describe the interplay between electronic and lattice degrees of freedom was augmented by an anharmonic phonon–phonon coupling describing the interaction between the triatomic O–Sr–O molecular vibration and the independent apical phonons located on the Oap sites. This extra term reads

$$H_{Sr} = K \left(\beta^\dagger b_L b_R + \beta b_L^\dagger b_R^\dagger \right), \quad (1)$$

where K is the strength of the anharmonic interaction between the independent Oap phonons, described by the creation (annihilation) operators b_i^\dagger (b_i), where $i = L, R$ stands for left (L) and right (R) apical oxygens in the cluster, as shown in figure 1, and the triatomic molecular phonon modes β^\dagger (β), associated with the locked vibration of the Oap–Sr–Oap chain in the dielectric layer. This anharmonic term is introduced in order to capture the dynamics associated with the Sr atom in the Cu–Oap IQTPs, as seen by the experimental results discussed above. The internal dynamics within this cluster defines the IQTP exchange as the oscillation of the excess charge and displacement on an Oap site via tunneling at a frequency higher than thermally activated hopping of the polaron to a neighboring site. This is accomplished by exchanging these characteristics with an adjacent, degenerate oxygen atom.

In addition to the exact diagonalization calculations, the charge–lattice dynamics was evaluated via the Kuramoto approach for synchronization of coupled oscillators by equating the anharmonic coupling K of the the O–Sr–O vibration to the coupling between phase oscillators in the Kuramoto model [64, 65]. In addition to its application here incorporating the EXAFS results, this approach has also been applied to the emergence of superconductivity as a synchronization problem [78]. The calculations shown here were performed by varying the anharmonic interaction strength, K , while fixing the electron–phonon coupling, λ , in the non-adiabatic regime that defines the cluster. This local electron–phonon coupling is present only on the apical positions Oap in order to ensure polaron formation. Further details of the exact diagonalization method and the Kuramoto analysis can be found in [30, 31].

The diagonalization procedure, incorporated with the synchronization driven by anharmonicity via the Kuramoto model, showed that at a critical value of K , K_c , the system undergoes a first order transition, where the order parameter is written as

$$r = \sqrt{1 - \frac{K}{rK_c}}. \quad (2)$$

The transition is also defined by discontinuities in the density of charges on the oxygen ions, namely the two apical oxygens, $n_{el}(O_{ap})$, the planar oxygen site, $n_{el}(O_{pl})$, and the tunneling frequency, $\hbar\omega_T = E_1 - E_0$, the difference in energy between the ground and first excited states, as summarized in figure 6. The Kuramoto analysis shows that this transition can be understood as a dynamic synchronization; when $K > K_c$ correlated, anti-phase tunneling of the two Cu–Oap pairs is initiated between their opposite configurations of displacement and charge.

For $K < K_c$, the unsynchronized phase, the excess charge is localized on either the left or right Oap due to the strong local electron–phonon coupling, forming two separated potential wells (figure 7(a)), between which no tunneling occurs. When the system transforms to the synchronized, phase-locked state, the resulting delocalization of the charge transfers a fraction of

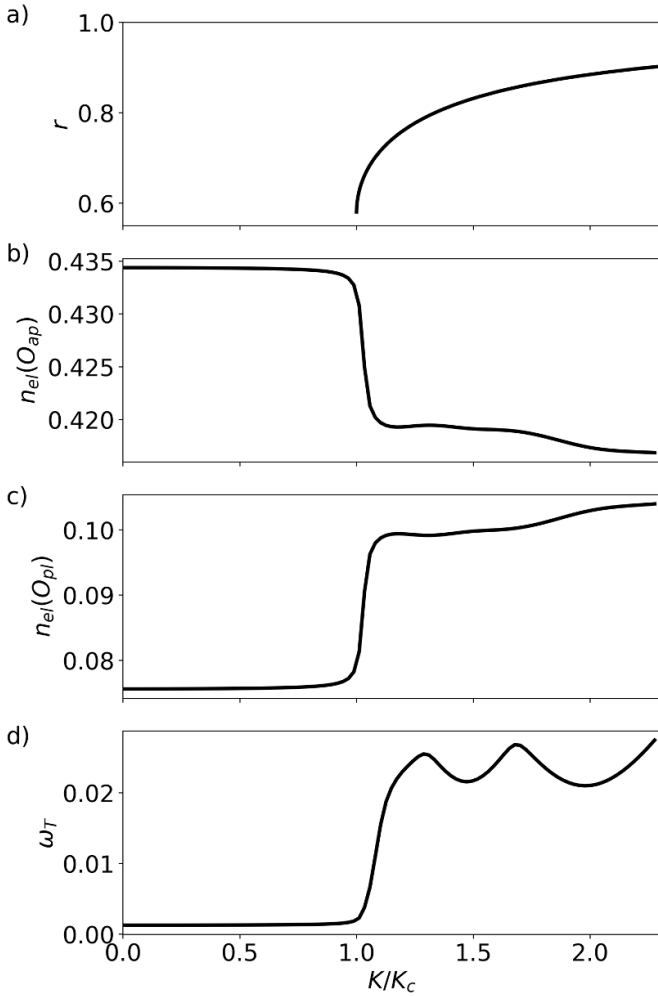


Figure 6. K dependence of cluster characteristics. (a) Order parameter for synchronization of IQTPs within the Kuramoto model as in equation (2). (b) Excess hole density on each Oap. (c) Excess hole density on Opl. (d) Tunneling frequency associated with the IQTPs in units of the electronic hopping parameter.

the excess charge originally on the two Oap atoms to Opl. The synchronization extends the wave function to form this third local minimum on Opl (figure 7(a)) and collapses the energy levels so that the excitation energies are greatly reduced. This delocalization and dispersion throughout the cluster of the hole that started on a single Oap is a clear signature that the synchronization of the IQTPs through the anharmonic Oap–Sr–Oap phonon modifies the electronic properties of the entire system. The resulting triple-well functions as an anharmonic-structural-adiabatic-passage promoting charge delocalization, that once formed may further enhance the oscillator synchronization in a positive feedback loop. Using the example of the polaronic tunneling frequency, $\hbar\omega_T$ (figure 6(d)), it is seen that at K values below the critical value K_c , $\hbar\omega_T = 0$, no tunneling occurs and the polarons are trapped on their original left or right sites. Above K_c the abrupt increase in $\hbar\omega_T$ is the signature of the transition to the synchronized phase. Because it is essentially a spectroscopic parameter, an interesting aspect of ω_T is the structure in the synchronized phase above K_c (figure 6(d))

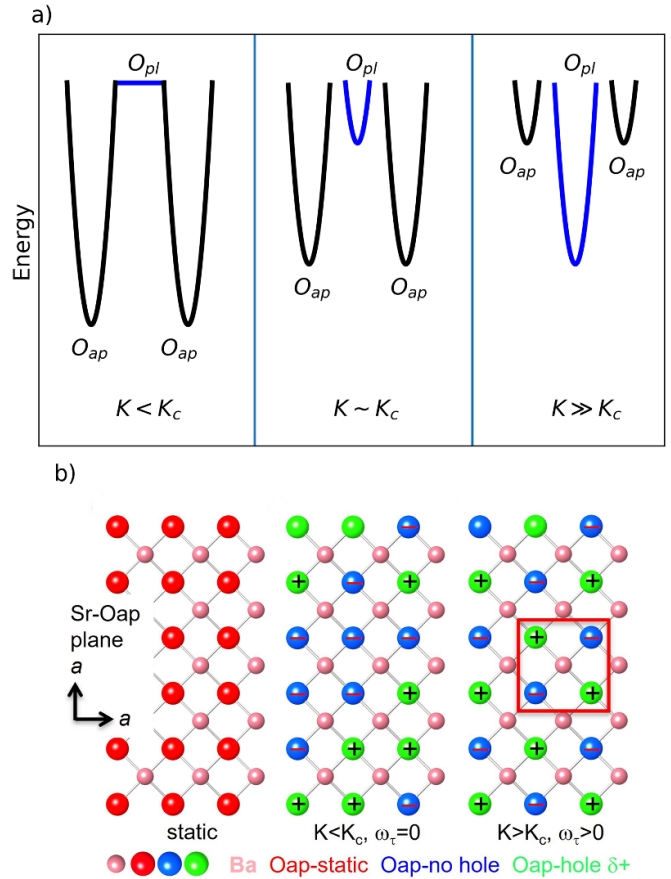


Figure 7. Charge distributions. (a) Density of excess hole on the two Oap and Opl in three regimes for different K values. Prior to synchronization, the hole resides on either one of the two Oap atoms. As K increases, starting at the initiation of the IQTP synchronization at $K \sim K_c$, increasing amounts of hole density are transferred to Opl. (b) Schematic of dielectric, Sr-Oap layer in the ab plane. In the static structure, all of the Oap are in the same crystallographic position. In the instantaneous or dynamic structure for $K < K_c$, in this snapshot half of the oxygen atoms are randomly distributed at the site with the longer Cu–O distance (green, +) and the other half exhibit the shorter Cu–O distance (blue, ‘-’). For $K > K_c$, in the synchronized phase, the ratio is the same but now a snapshot of the Oap atoms shows alternating up and down to double the unit cell size of the dynamic structure. This structure exhibits d symmetry about the Sr ion at the center of the CuO_2 squares.

that is caused by avoided crossings in the ground to excited state transition. Such structure does not occur in the other parameters.

5. Discussion and conclusion

Comparisons of the Cu–Sr and Cu–Oap contributions to the Cu K EXAFS of YSCO–Mo and SCO over their transition temperatures demonstrated very strong coupling of the local charge-lattice dynamics within the entire dielectric layer to their superconductivity. Since the two-site distributions of the Cu–Oap distributions constitute the IQTPs in these compounds, the high degree of correlation between the $\chi(R)$ moduli amplitudes for both neighbors over the full temper-

ature range and abrupt changes across the transition further established a strong, three-way coupling between the Cu–Sr anharmonic distributions, the IQTPs, and the superconductivity in both materials despite the very different structures of their Cu–O sublattices. This three-way correlation implies that even without the direct participation of the Sr^{2+} in the charge dynamics, its local dynamic structure is a component of the unusual electronic properties of these cuprate compounds. The novel extension of the IQTP imposed by the experimental results is the anharmonic coupling of the Oap of the IQTPs to the Sr^{2+} ion forming the tri-atomic chain Oap–Sr–Oap of the cluster. Far from being passive [56], our calculations demonstrate that this coupling and consequent synchronized, anti-phase motions of the Oap atoms and their associated charges have substantial effects on the dynamics and charge distributions in the other domains of the materials, notably the CuO_2 planes where the charge on the oxygen is highly correlated with T_c [79]. The extension of the localized wave function on Oap to multiple IQTPs and sites in the CuO_2 plane promotes electron–electron interactions that go far beyond the acknowledged special role of the Oap atom in controlling the carrier density [79–81] or, in the extreme case, the suggestion that pairing could occur through possible lateral vibrations [55] (although these are not observed in EXAFS). Furthermore, depending on the details of short- and long-range interactions between IQTPs, assemblies of finite densities of them will likely result in mesoscopic patterns, including clusters and stripes, and possibly dynamical charge density waves (CDW) [82]. However, given the importance of specific nonlinear and nonadiabatic degree-of-freedom that we have identified for our 6-atom single IQTP, conventional CDW descriptions are unlikely to be directly relevant. The synchronization proffered by the anharmonically coupled two-site distributions of the IQTPs therefore also entangles at least some of the relevant degrees of freedom between the conduction and dielectric layers and charge reservoirs.

A persisting problem with EXAFS of highly correlated systems including cuprates is integrating its information on the behavior of specific atoms pairs with other spectroscopic data that are ensemble averages. This is often exacerbated by its sensitivity to the dynamic structure that can cause certain results to contradict the more intuitive ones from crystallography. In contrast to the immediate utility of chemical speciation that is defined by local structure, the interpretation of many experiments in terms of reciprocal space quantities means that there is no simple transformation from, for example, phonon spectra to anomalies in the real space pair distributions identified by EXAFS. In their obvious demonstration of coupling between charge fluctuations, phonons, and pairing-HTSC our results here are complementary with recent reports on RIXS [82–85] where the characterization of several excitations came to the same conclusions about charge dynamics. However, the different dependence on temperature and locations within the structures show that the phenomena probed by these measurements are not the same. This problem with unifying data from diverse sources is not unique to EXAFS. The difficulty of incorporating disparate results from multiple experiments into a coherent picture is a major factor in the continued absence of an

HTSC theory. In terms of overcoming instead of contributing to this dilemma, an often-overlooked fact from the EXAFS of IQTPs is relevant; the two-site distribution of the apical oxygen atoms applies to every one of those atoms in the entire crystal, a signal from a third oxygen that is not participating in an IQTP is not found. If the local charge fluctuations are in fact universal, then the different electronic phases including HTSC might originate in their organization and collective behavior.

These experimental and theoretical results provide a critical extension to our prior EXAFS studies that demonstrated that the two-site Cu–O distributions in the dynamic structure that constitute the IQTPs are strongly coupled to the HTSC [6, 8, 12, 13, 19, 30, 31] as well as these overdoped, superconducting SCO and YSCO–Mo [57]. It would be expected that a phenomenon that is coupled to the HTSC mechanism would exhibit a correlation with T_c . Such behavior has been reported for the Cu–O bond lengths, and the hole density on the oxygen atoms [79, 86] that is analogous to the charge transfer caused by the synchronization. The observed variability in the type and extent of the IQTPs in materials with similar critical temperatures could therefore seem to minimize their importance. This argument based on isolating microscopic components of the material is countered by the increased complexity of the IQTPs we have reported here. In contrast to our original description of an IR phonon acting on a Cu–Oap pair, the entity of interest consists of not only the phonon giving the two-site distribution, but now also the anharmonic one connecting the Oap to the strontium that, when the coupling exceeds a threshold strength, synchronizes them over all of the copper and Oap in an entire domain, including the Opl, to which hole density is transferred, all of which are entangled. A simple linear relationship between all of these parameters defining the IQTPs and the HTSC would only occur if the coupling between each of them was weak, which these results show is not the case.

In addition to the challenges to existing theories posed by the HPO phase diagram, the differences between the structures of YSCO–Mo and SCO, the effects of the excess oxygen atoms on T_c , and the details of their IQTPs merit notice in their own right. In the search for a common factor in HTSC cuprates, the totality of the dynamic structure measurements indicate that strong coupling of the anharmonic, dynamic structure of Cu–Sr and IQTPs to each other and the HTSC is universal among all of the materials studied. However, the details in terms of the atoms involved, their locations in the lattice, and their displacements caused by the exchange can exhibit large variations, possibly even within different preparations of the same compound. These new EXAFS measurements greatly extend the range of the structure and behavior of IQTPs beyond the previously observed partial collapse of the double well potential near the HTSC transition. Not only are the two minima of the double well potential non-degenerate, but also the difference in their energies varies across the entire temperature range with a large shift at the superconducting transition even while their separation is unchanged. The essential factor in the HTSC-IQTP coupling is therefore not limited to the equal splitting in the dynamic structure of the Oap sites into

a two-site distribution along the c axis with tunneling frequencies on the order of 100 cm^{-1} . The coupling can also manifest itself in the dynamic structure as double well potentials and their associated charge dynamics that display other values of the two energies, locations in the lattice, and responses to the HTSC transition.

A critical aspect for identifying and characterizing the IQTPs is the experimental signatures. As with HPO cuprates, dynamic structure is a topic that has not been thoroughly examined by the community, especially inelastic neutron pdf measurements. There has been much more continuity with EXAFS, but the absence of theoretical bases for both the origins of the dynamical multisite distributions and their effects on properties of interest that are the intersection of the local coordination chemistry with the physics have impeded the utilization of its findings. Recent improvements in the measurements that result in the much larger number of higher quality spectra provide the new evidence here, e.g. the contrast between the absence of any significant temperature dependence in the total spectra of figure 2(a) and the large change at the superconducting transition well above the noise level in the isolated Cu–Oap contribution. We have already initiated a more thorough evaluation of IQTPs by applying these techniques to the more conventional HTSC materials.

The role of electron–phonon coupling in the HTSC has been mapped to that of certain phonons, for example the B_{1g} phonon that is the antiphase buckling of the Cu–O–Cu moieties of the CuO_2 plane [52], was shown shortly after the discovery of HTSC [22, 87], although there is disagreement on the strength of its coupling to the HTSC [88]. Anomalies in phonon dispersions indicative of strong electron–phonon coupling that are correlated with both T_c and the doping, e.g. the giant softening of the bond-stretching phonon frequencies off of the zone center caused by strong renormalization along [010] and [100] directions and avoided crossings, are a common characteristic of cuprates [45–48, 89]. Although these are still insufficient to cause HTSC, insofar as the doping-induced charge inhomogeneities are localized [90, 91], the widths of the phonon peaks reflect their resulting wide range of energies [92]. The comparison of the doping dependence of these $\sim 70 \text{ meV}$ phonon dispersion anomalies with the ‘kink’ in angle-resolved photoemission denotes different origins for these two spectral signatures. Whereas this feature in ARPES would indicate electron-anomalous phonon coupling, its presence in neutron scattering would result from collective charge excitations [48, 93] that could promote a novel HTSC mechanism. This would be a likely description of an important role for a synchronized IQTP phase that directly combines both lattice and charge dynamics sufficiently large to involve exchange among different sites. Although there are no zone center phonons with the antiphase displacements of the synchronized phase of the IQTPs, analogous to the neutron scattering, the correlated Cu–Oap motions could originate from a phonon not belonging to the Brillouin zone center. Utilizing the $\text{YBa}_2\text{Cu}_3\text{O}_7$ (YBCO)-type structure (figure 1(c)), the calculated atomic displacements are described by a symmetry-adapted coordinate belonging to the X_2 -irreducible representation at the X point of the tetragonal Brillouin zone, where







only one branch of the $q = (0 \ 1/2 \ 0)$ phonon mode is involved. This off zone-center phonon exhibits the same d -symmetry with respect to the centers of the CuO_2 squares as the extended synchronized regime for the IQTP’s, as shown in figure 7(b).

Summarizing, in a doped system with the appropriate combination of parameters and relative energies of the transition metal and oxygen states, the IQTPs are a natural outcome of coupling this phonon to the coordination chemistry of the transition metal ions and the preferred geometries associated with their valence. This arises from the necessary mix of ionic and covalent character in the Cu–O bond, that also has two species possessing metal–oxygen bonds separated by a barrier of requisite height and width. The partial localization of the charge causes the metal sites to adopt these geometries and bond lengths within the lattice. This would give the known sensitivity to the interatomic distances and angles [94, 95]. If the thermal motion of the Cu–O pair traverses this range, then instead of the potential being featureless it can evolve into the two-site distribution by developing distinct local minima at those locations corresponding to the preferred charge distributions and their bonding modes. Overall, these EXAFS results combined with the theoretical developments on the physics of synchronized IQTPs can provide a new route to the understanding of induced electron–electron interactions in high-temperature cuprate superconductors.

Data availability statement

All data that support the findings of this study are included within the article (and any supplementary files).

ORCID iDs

Victor Velasco  <https://orcid.org/0000-0003-3904-8602>
 Marcello B Silva Neto  <https://orcid.org/0000-0002-6817-3472>
 Andrea Gauzzi  <https://orcid.org/0000-0002-4159-1383>
 Maarit Karppinen  <https://orcid.org/0000-0003-1091-1169>
 Sandro Wimberger  <https://orcid.org/0000-0002-8433-1733>
 Gianguido Baldinozzi  <https://orcid.org/0000-0002-6909-0716>

References

- [1] Bednorz J G and Muller K A 1986 Possible high T_c superconductivity in the Ba–La–Cu–O system *Z. Phys. B* **64** 189–93
- [2] Mitrano M *et al* 2018 Anomalous density fluctuations in a strange metal *Proc. Natl Acad. Sci. USA* **115** 5392–6
- [3] Bozovic I, He X, Wu J and Bollinger A T 2018 The vanishing superfluid density in cuprates—and why it matters *J. Supercond. Nov. Magn.* **31** 2683–90
- [4] Bishop A R 2020 A lattice litany for transition metal oxides *Condens. Matter* **5** 46
- [5] Zhou X J, Lee W-S, Imada M, Trivedi N, Phillips P, Kee H-Y, Törmä P and Eremets M 2021 High-temperature superconductivity *Nat. Rev. Phys.* **3** 462–5

- [6] Conradson S D, Raistrick I D and Bishop A R 1990 Axial oxygen centered lattice instabilities and high-temperature superconductivity *Science* **248** 1394–8
- [7] Deleon J M, Conradson S D, Batistic I and Bishop A R 1990 Evidence for an axial oxygen-centered lattice fluctuation associated with the superconducting transition in $\text{YBa}_2\text{Cu}_3\text{O}_7$ *Phys. Rev. Lett.* **65** 1675–8
- [8] Allen P G, Deleon J M, Conradson S D and Bishop A R 1991 Characterization of a split axial-oxygen site in $\text{TlBa}_2\text{Ca}_3\text{Cu}_4\text{O}_{11}$ by extended x-ray-absorption fine-structure spectroscopy *Phys. Rev. B* **44** 9480–5
- [9] Deleon J M, Conradson S D, Batistic I and Bishop A R 1991 Correlation between axial-oxygen anharmonicity and T_c in $\text{YBa}_2\text{Cu}_3\text{O}_7$ and related-compounds *Phys. Rev. B* **44** 2422–5
- [10] Deleon J M, Batistic I, Bishop A R, Conradson S D and Trugman S A 1992 Polaron origin for anharmonicity of the axial oxygen in $\text{YBa}_2\text{Cu}_3\text{O}_7$ *Phys. Rev. Lett.* **68** 3236–9
- [11] Deleon J M *et al* 1992 Axial oxygen-centered lattice instabilities in $\text{YBa}_2\text{Cu}_3\text{O}_7$ —an application of the analysis of extended x-ray-absorption fine-structure in anharmonic systems *Phys. Rev. B* **45** 2447–57
- [12] Deleon J M, Li G G, Conradson S D, Bishop A R, Subramanian M A and Raistrick I D 1994 Planar oxygen-centered lattice instabilities in Tl-based high-temperature superconductors *Physica C* **220** 377–82
- [13] Booth C H *et al* 1996 Comparison of local structure measurements from *c*-axis polarized XAFS between a film and a single crystal of $\text{YBa}_2\text{Cu}_3\text{O}_{7-\delta}$ as a function of temperature *Phys. Rev. B* **54** 9542–54
- [14] DeLeon J M *et al* 1996 X-ray absorption fine structure applied to the study of systems with lattice instabilities *Applications of Synchrotron Radiation Techniques to Materials Science III* vol 437, ed L J Terminello, S M Mini, H Ade and D L Perry (Cambridge University Press) pp 189–99
- [15] Conradson S D, DeLeon J M and Bishop A R 1997 Local phase separation in Tl-based oxide superconductors *J. Supercond.* **10** 329–32
- [16] Acosta-Alejandra M, de Leon J M, Conradson S D and Bishop A R 2002 Evidence for a local structural change in $\text{La}_2\text{CuO}_{4.1}$ across the superconducting transition *J. Supercond.* **15** 355–60
- [17] Campi G and Bianconi A 2005 Complex phase separation in oxygen-doped cuprates $\text{La}_2\text{CuO}_{4+y}$ superconductors *J. Supercond.* **18** 637–42
- [18] de Leon J M, Acosta-Alejandra M, Conradson S D and Bishop A R 2008 Change of the in-plane Cu–O bond distribution in $\text{La}_2\text{CuO}_{4.1}$ across T_c *J. Phys. Chem. Solids* **69** 2288–91
- [19] Zhang C J and Oyanagi H 2009 Local lattice instability and superconductivity in $\text{La}_{1.85}\text{Sr}_{0.15}\text{Cu}_{1-x}\text{M}_x\text{O}_4$ ($M = \text{Mn}, \text{Ni}$ and Co) *Phys. Rev. B* **79** 064521
- [20] Oyanagi H, Zhang C, Tsukada A and Naito M 2009 Lattice instability in high-temperature superconducting cuprates: polarons probed by EXAFS *J. Supercond. Nov. Magn.* **22** 165–8
- [21] Egami T *et al* 1991 Local structural anomaly near T_c observed by pulsed neutron-scattering *Physica C* **185** 867–8
- [22] Arai M, Yamada K, Hosoya S, Hannon A C, Hidaka Y, Taylor A D and Endoh Y 1994 Local structural instability of high- T_c oxide superconductors studied by inelastic neutron-scattering *J. Supercond.* **7** 415–8
- [23] Menushenkov A P and Klementev K V 2000 Extended x-ray absorption fine-structure indication of a double-well potential for oxygen vibration in $\text{Ba}_{1-x}\text{K}_x\text{BiO}_3$ *J. Phys.: Condens. Matter* **12** 3767–86
- [24] Menushenkov A P, Klementev K V, Konarev P V, Meshkov A A, Benazeth S and Purans J 2000 The double-well oscillating potential of oxygen atoms in perovskite system $\text{Ba}(\text{K})\text{BiO}_3$: EXAFS—analysis results *Nucl. Instrum. Methods Phys. Res. A* **448** 340–4
- [25] Salkola M I, Bishop A R, Deleon J M and Trugman S A 1994 Dynamic polaron tunneling in $\text{YBa}_2\text{Cu}_3\text{O}_7$ —optical-response and inelastic neutron-scattering *Phys. Rev. B* **49** 3671–4
- [26] Salkola M I, Bishop A R, Trugman S A and Deleon J M 1995 Correlation-function analysis of nonlinear and nonadiabatic systems—polaron tunneling *Phys. Rev. B* **51** 8878–91
- [27] Bishop A R, Mihailovic D and de Leon J M 2003 Signatures of mesoscopic Jahn–Teller polaron inhomogeneities in high-temperature superconductors *J. Phys.: Condens. Matter* **15** L169–75
- [28] Chen C-C, Sentef M, Kung Y F, Jia C J, Thomale R, Moritz B, Kampf A P and Devereaux T P 2013 Doping evolution of the oxygen K-edge x-ray absorption spectra of cuprate superconductors using a three-orbital Hubbard model *Phys. Rev. B* **87** 165144
- [29] Chen Y-J, Jiang M G, Luo C W, Lin J-Y, Wu K H, Lee J M, Chen J M, Kuo Y K, Juang J Y and Mou C-Y 2013 Doping evolution of Zhang–Rice singlet spectral weight: a comprehensive examination by x-ray absorption spectroscopy *Phys. Rev. B* **88** 134525
- [30] Velasco V, Silva Neto M B, Perali A, Wimberger S, Bishop A R and Conradson S D 2021 Evolution of charge-lattice dynamics across the Kuramoto synchronization phase diagram of quantum tunneling polarons in cuprate superconductors *Condens. Matter* **6** 52
- [31] Velasco V, Silva Neto M B, Perali A, Wimberger S, Bishop A R and Conradson S D 2022 Kuramoto synchronization of quantum tunneling polarons for describing the structure in cuprate superconductors *Phys. Rev. B* **105** 174305
- [32] Dahm T, Hinkov V, Borisenko S V, Kordyuk A A, Zabolotnyy V B, Fink J, Büchner B, Scalapino D J, Hanke W and Keimer B 2009 Strength of the spin-fluctuation-mediated pairing interaction in a high-temperature superconductor *Nat. Phys.* **5** 217–21
- [33] Giannetti C *et al* 2016 Ultrafast optical spectroscopy of strongly correlated materials and high-temperature superconductors: a non-equilibrium approach *Adv. Phys.* **65** 58–238
- [34] Stewart G R 2017 Unconventional superconductivity *Adv. Phys.* **66** 75–196
- [35] Merritt A M *et al* 2019 Low-energy phonons in $\text{Bi}_2\text{Sr}_2\text{CaCu}_2\text{O}_{8+\delta}$ and their possible interaction with electrons measured by inelastic neutron scattering *Phys. Rev. B* **100** 144502
- [36] O’Mahony S M, Ren W, Chen W, Chong Y X, Liu X, Eisaki H, Uchida S, Hamidian M H and Davis J C S 2022 On the electron pairing mechanism of copper-oxide high temperature superconductivity *Proc. Natl Acad. Sci. USA* **119** 2207449119
- [37] Anzai H, Arita M, Namatame H, Taniguchi M, Ishikado M, Fujita K, Ishida S, Uchida S and Ino A 2017 A new landscape of multiple dispersion kinks in a high- T_c cuprate superconductor *Sci. Rep.* **7** 4830
- [38] He Y *et al* 2018 Rapid change of superconductivity and electron–phonon coupling through critical doping in Bi-2212 *Science* **362** 62–65
- [39] He Y *et al* 2018 Persistent low-energy phonon broadening near the charge-order *q* vector in the bilayer cuprate $\text{Bi}_2\text{Sr}_2\text{CaCu}_2\text{O}_{8+\delta}$ *Phys. Rev. B* **98** 035102
- [40] Li Z-X, Kivelson S A and Lee D-H 2021 Superconductor-to-metal transition in overdoped cuprates *npj Quantum Mater.* **6** 36

- [41] Sobota J A, He Y and Shen Z X 2021 Angle-resolved photoemission studies of quantum materials *Rev. Mod. Phys.* **93** 025006
- [42] Ideta S *et al* 2021 Hybridization of Bogoliubov quasiparticles between adjacent CuO₂ layers in the triple-layer cuprate Bi₂Sr₂CaCu₂O_{8+δ} studied by angle-resolved photoemission spectroscopy *Phys. Rev. Lett.* **127** 217004
- [43] Yan H *et al* 2023 Ubiquitous coexisting electron-mode couplings in high-temperature cuprate superconductors *Proc. Natl Acad. Sci. USA* **120** e2219491120
- [44] Kovaleva N N *et al* 2004 *c*-axis lattice dynamics in Bi-based cuprate superconductors *Phys. Rev. B* **69** 054511
- [45] Pintschovius L *et al* 2004 Oxygen phonon branches in YBa₂Cu₃O₇ *Phys. Rev. B* **69** 214506
- [46] Pintschovius L, Reznik D and Yamada K 2006 Oxygen phonon branches in overdoped La_{1.7}Sr_{0.3}Cu₃O₄ *Phys. Rev. B* **74** 174514
- [47] Reznik D, Pintschovius L, Ito M, Iikubo S, Sato M, Goka H, Fujita M, Yamada K, Gu G D and Tranquada J M 2006 Electron–phonon coupling reflecting dynamic charge inhomogeneity in copper oxide superconductors *Nature* **440** 1170–3
- [48] Park S R *et al* 2014 Evidence for a charge collective mode associated with superconductivity in copper oxides from neutron and x-ray scattering measurements of La_{2–x}Sr_xCuO₄ *Phys. Rev. B* **89** 020506
- [49] Braicovich L *et al* 2020 Determining the electron–phonon coupling in superconducting cuprates by resonant inelastic x-ray scattering: methods and results on Nd_{1+x}Ba_{2–x}Cu₃O_{7–δ} *Phys. Rev. Res.* **2** 023231
- [50] Huang E W *et al* 2021 Extracting correlation effects from momentum-resolved electron energy loss spectroscopy: synergistic origin of the dispersion kink in Bi_{2.1}Sr_{1.9}CaCu₂O_{8+x} *Phys. Rev. B* **103** 035121
- [51] Peng Y Y *et al* 2022 Doping dependence of the electron–phonon coupling in two families of bilayer superconducting cuprates *Phys. Rev. B* **105** 115105
- [52] Johnston S, Vernay F, Moritz B, Shen Z-X, Nagaosa N, Zaanen J and Devereaux T P 2010 Systematic study of electron–phonon coupling to oxygen modes across the cuprates *Phys. Rev. B* **82** 064513
- [53] Ohgoe T and Imada M 2017 Competition among superconducting, antiferromagnetic and charge orders with intervention by phase separation in the 2D Holstein–Hubbard model *Phys. Rev. Lett.* **119** 197001
- [54] Kim S, Chen X, Fitzhugh W and Li X 2018 Apical charge flux-modulated in-plane transport properties of cuprate superconductors *Phys. Rev. Lett.* **121** 157001
- [55] Rosenstein B and Shapiro B Y 2021 Apical oxygen vibrations dominant role in d-wave cuprate superconductivity and its interplay with spin fluctuations *J. Phys. Commun.* **5** 055013
- [56] Bozin E S *et al* 2016 Charge-screening role of *c*-axis atomic displacements in YBa₂Cu₃O_{6+x} and related superconductors *Phys. Rev. B* **93** 054523
- [57] Conradson S D *et al* 2020 Nonadiabatic coupling of the dynamical structure to the superconductivity in YSr₂Cu_{2.75}Mo_{0.25}O_{7.54} and Sr₂CuO_{3.3} *Proc. Natl Acad. Sci. USA* **117** 33099–106
- [58] Conradson S D, Geballe T H, Jin C, Cao L, Baldinozzi G, Jiang J M, Latimer M J and Mueller O 2020 Local structure of Sr₂CuO_{3.3}, a 95 K cuprate superconductor without CuO₂ planes *Proc. Natl Acad. Sci. USA* **117** 4565–70
- [59] Conradson S D *et al* 2020 Local lattice distortions and dynamics in extremely overdoped superconducting YSr₂Cu_{2.75}Mo_{0.25}O_{7.54} *Proc. Natl Acad. Sci. USA* **117** 4559–64
- [60] Arai M, Yamada K, Hidaka Y, Itoh S, Bowden Z A, Taylor A D and Endoh Y 1992 Anomaly of phonon state of superconducting YBa₂Cu₃O₇ studied by inelastic neutron-scattering *Phys. Rev. Lett.* **69** 359–62
- [61] Oh D, Song D, Kim Y, Miyasaka S, Tajima S, Bok J M, Bang Y, Park S R and Kim C 2021 B-1g-phonon anomaly driven by fermi surface instability at intermediate temperature in YBa₂Cu₃O_{7–δ} *Phys. Rev. Lett.* **127** 277001
- [62] Gao W B *et al* 2009 Out-of-plane effect on the superconductivity of Sr_{2–x}Ba_xCuO_{3+δ} with *T_c* up to 98 K *Phys. Rev. B* **80** 094523
- [63] Haskel D, Stern E A, Hinks D G, Mitchell A W and Jorgensen J D 1997 Altered Sr environment in La_{2–x}Sr_xCuO₄ *Phys. Rev. B* **56** R521–4
- [64] Kuramoto Y 1975 Self-entrainment of a population of coupled non-linear oscillators *Int. Symp. on Mathematical Problems in Theoretical Physics* ed H Araki (Springer, Kyoto University) p 420
- [65] Kuramoto Y and Nishikawa I 1987 Statistical macrodynamics of large dynamical-systems—case of a phase-transition in oscillator communities *J. Stat. Phys.* **49** 569–605
- [66] Gauzzi A *et al* 2016 Bulk superconductivity at 84 K in the strongly overdoped regime of cuprates *Phys. Rev. B* **94** 180509
- [67] Liu Q Q *et al* 2006 Enhancement of the superconducting critical temperature of Sr₂CuO_{3+δ} up to 95 K by ordering dopant atoms *Phys. Rev. B* **74** 100506(R)
- [68] Yang H, Liu Q Q, Li F Y, Jin C Q and Yu R C 2006 Structure and microstructure of superconductor Sr₂CuO_{3+δ} (nominal δ = 0.4) prepared under high pressure *Supercond. Sci. Technol.* **19** 934–40
- [69] Sederholm L, Conradson S D, Geballe T H, Jin C-Q, Gauzzi A, Gilioli E, Karppinen M and Baldinozzi G 2021 Extremely overdoped superconducting cuprates via high pressure oxygenation methods *Condens. Matter* **6** 50
- [70] Tomioka Y, Naito M, Kishio K and Kitazawa K 1994 The Meissner and shielding effects of high-temperature oxide superconductors *Physica C* **223** 347
- [71] Felner I 1998 The effect of grains size and temperature on superconducting parameters *J. Therm. Anal. Calorimetry* **52** 447
- [72] Smolyak B M, Postrekhin E V and Ermakov G V 1994 ZFC, FC and REM susceptibility of granular superconductors *Supercond. Sci. Technol.* **7** 427
- [73] Dollase W A 1986 Correction of intensities for preferred orientation in powder diffractometry—application of the march model *J. Appl. Crystallogr.* **19** 267–72
- [74] Conradson S D, Manara D, Wastin F, Clark D L, Lander G H, Morales L A, Rebizant J and Rondinella V V 2004 Local structure and charge distribution in the UO₂–U₄O₉ system *Inorg. Chem.* **43** 6922–35
- [75] Conradson S D *et al* 2014 Nanoscale heterogeneity, premartensitic nucleation and a new plutonium structure in metastable delta fcc Pu–Ga alloys *Phys. Rev. B* **89** 224102
- [76] Conradson S D *et al* 2014 Intrinsic nanoscience of δ Pu–Ga alloys: local structure and speciation, collective behavior, nanoscale heterogeneity and aging mechanisms *J. Phys. Chem. C* **118** 8541–63
- [77] Bunker G 1983 Application of the ratio method of EXAFS analysis to disordered systems *Nucl. Instrum. Methods Phys. Res.* **207** 437–44
- [78] Velasco V and Neto M B S 2021 Unconventional superconductivity as a quantum Kuramoto synchronization problem in random elasto-nuclear oscillator networks *J. Phys. Commun.* **5** 015003
- [79] Rybicki D, Jurkutat M, Reichardt S, Kapusta C and Haase J 2016 Perspective on the phase diagram of cuprate high-temperature superconductors *Nat. Commun.* **7** 11413
- [80] Sahiner A, Crozier E D, Jiang D T and Ingalls R 1999 Pressure-induced bond buckling in YBa₂Cu₃O_{7–δ} *Phys. Rev. B* **59** 3902–10

- [81] Chen X, Dong J and Li X 2020 A picture of pseudogap phase related to charge fluxes *npj Comput. Mater.* **6** 103
- [82] Arpaia R *et al* 2019 Dynamical charge density fluctuations pervading the phase diagram of a Cu-based high- T_c superconductor *Science* **365** 906
- [83] Yu B *et al* 2020 Unusual dynamic charge correlations in simple-tetragonal $\text{HgBa}_2\text{CuO}_{4+\delta}$ *Phys. Rev. X* **10** 021059
- [84] Huang H Y *et al* 2021 Quantum fluctuations of charge order induce phonon softening in a superconducting cuprate *Phys. Rev. X* **11** 041038
- [85] Arpaia R *et al* 2023 Signature of quantum criticality in cuprates by charge density fluctuations *Nat. Commun.* **14** 7198
- [86] Jurkutat M, Avramovska M, Williams G V M, Dernbach D, Pavićević D and Haase J 2019 Phenomenology of Cu-63 nuclear relaxation in cuprate superconductors *J. Supercond. Nov. Magn.* **32** 3369–76
- [87] Devereaux T P, Virosztek A and Zawadowski A 1995 Charge-transfer fluctuation, d-wave superconductivity and the B-1g Raman phonon in cuprates *Phys. Rev. B* **51** 505–14
- [88] Raichle M *et al* 2011 Highly anisotropic anomaly in the dispersion of the copper-oxygen bond-bending phonon in superconducting $\text{YBa}_2\text{Cu}_3\text{O}_7$ from inelastic neutron scattering *Phys. Rev. Lett.* **107** 177004
- [89] Reznik D, Pintschovius L, Tranquada J M, Arai M, Endoh Y, Masui T and Tajima S 2008 Temperature dependence of the bond-stretching phonon anomaly in $\text{YBa}_2\text{Cu}_3\text{O}_{6.95}$ *Phys. Rev. B* **78** 094507
- [90] Singer P M, Imai T, Chou F C, Hirota K, Takaba M, Kakeshita T, Eisaki H and Uchida S 2005 ^{17}O NMR study of the inhomogeneous electronic state in $\text{La}_{2-x}\text{Sr}_x\text{CuO}_4$ crystals *Phys. Rev. B* **72** 014537
- [91] Chen W, Khaliullin G and Sushkov O P 2009 Coulomb disorder effects on angle-resolved photoemission and nuclear quadrupole resonance spectra in cuprates *Phys. Rev. B* **80** 094519
- [92] Park S R, Hamann A, Pintschovius L, Lamago D, Khaliullin G, Fujita M, Yamada K, Gu G D, Tranquada J M and Reznik D 2011 Effects of charge inhomogeneities on elementary excitations in $\text{La}_{2-x}\text{Sr}_x\text{CuO}_4$ *Phys. Rev. B* **84** 214516
- [93] Park S R, Cao Y, Wang Q, Fujita M, Yamada K, Mo S-K, Dessau D S and Reznik D 2013 Broken relationship between superconducting pairing interaction and electronic dispersion kinks in $\text{La}_{2-x}\text{Sr}_x\text{CuO}_4$ measured by angle-resolved photoemission *Phys. Rev. B* **88** 220503
- [94] Chmaissem O, Jorgensen J D, Short S, Knizhnik A, Eckstein Y and Shaked H 1999 Scaling of transition temperature and CuO_2 plane buckling in a high-temperature superconductor *Nature* **397** 45–48
- [95] Agrestini S, Saini N L, Bianconi G and Bianconi A 2003 The strain of CuO_2 lattice: the second variable for the phase diagram of cuprate perovskites *J. Phys. A: Math. Gen.* **36** 9133–42